Journal of Molecular Graphics and Modelling 72 (2017) 88–95

Contents lists available at ScienceDirect

Journal of Molecular Graphics and Modelling

journal homepage: www.elsevier.com/locate/JMGM

Topical Perspectives

Identification of novel PAD4 inhibitors based on a pharmacophore model derived from transition state coordinates

Yu Wei[a,1], Ruihua Liu[c,1], Cui Liu[b,1], Jin Jin[a,**], Dongmei Li[a,**], Jianping Lin[a,b,*]

[a] State Key Laboratory of Medicinal Chemical Biology, College of Pharmacy and Tianjin Key Laboratory of Molecular Drug Research, Nankai University, Haihe Education Park, 38 Tongyan Road, Tianjin 300353, China
[b] Biodesign Center, Tianjin Institute of Industrial Biotechnology, Chinese Academy of Sciences, Tianjin 300308, China
[c] College of Life Sciences, Nankai University, Tianjin 300071, China

ARTICLE INFO

Article history:
Received 5 September 2016
Received in revised form 3 November 2016
Accepted 29 November 2016
Available online 19 December 2016

Keywords:
Protein arginine deiminases
Transition state
Molecular dynamic
Pharmacophore
Virtual screening

ABSTRACT

1.4 Protein arginine deiminases 4 (PAD4) is an attractive target for the development of novel and selective inhibitors of Rheumatoid Arthritis (RA). F-amidine is known as mechanism-based inhibitor targeting PAD4 and used as inactivators by covalently modifying the active site Cys645. To identify novel structural inhibitors of PAD4, we investigated the flexibility of protein on basis of the transition state geometry of PAD4 inhibited by F-amidine from our previous QM/MM calculation. And a pharmacophore model was generated containing four features (ADHH) using five representative structures from molecular dynamic (MD) simulation on basis of the transition state geometry of PAD4 inhibited by F-amidine. We performed virtual screening using the pharmacophore model and molecular docking methods, resulting in the discovery of two molecules with K_D (dissociation equilibrium constant) values of 112 μM and 218 μM against PAD4 through Surface Plasmon Resonance (SPR) experiments. These two molecules could potentially serve as PAD4 inhibitors.

1. Introduction

Protein Arginine Deiminases (PADs), including five known isoforms (PADs 1–4, and 6), catalyze the conversion of an arginine residue to a citrulline residue in humans [1,2]. The dysregulated modification of PADs often leads to severe human pathology diseases including Rheumatoid Arthritis (RA), colitis, and cancer [3]. In particular, dysregulated protein arginine deiminase 4 (PAD4) activity has been proven to promote the onset and progression of RA [4–6]. The current drugs of treatment in RA to data are to help relieve some of the symptoms including joint inflammation and pain and to prevent joint destruction and deformity [7]. Aspirin (Non-Steroidal Anti-Inflammatory Drugs, NSAIDs) and cortisone (corticosteroids), as fast-acting "first-line drugs", are used to reduce tissue pain and inflammation [8,9]. Methotremate (Rheumatrex, Trexall) and hydroxychloroquine (Plaquenil), as slow-acting "second-line drugs" or disease-modifying antirheumatic drugs (DMARDs), are used to promote disease remission and slow down the progression of disease [9–11]. However, there is no known cure for the underlying causes of the RA. Therefore, the identification and development of selective and more effective inhibitors for PAD4 remains necessary and urgent.

PAD4 consists of 663 amino acids with a molecular weight of 74 kDa and plays an important role in the epigenetics, which showed that the deamination of arginines on histones 3 and 4 can offer protection against arginine methylation [12]. PAD4 is a Ca^{2+} dependent enzyme, which can bind five calcium ions to stabilize the conformation of PAD4 and facilitates the binding of substrate [13]. Except for PAD6, the Ca^{2+} binding sites in PADs 1–4 are conserved [14]. Given PAD4's fundamental role in transcriptional regulation and causing RA, plenty of research and development work has attended to develop PAD4 inhibitors to regulate PAD4 activity and RA regression [15–22]. Most of the reversible inhibitors including taxol, streptomycin and minocycline are relatively weak inhibitors with millimolar IC_{50} values [16,17], except the GSK199 and GSK484 [15], the first highly potent PAD4-specific inhibitors with IC_{50} of 200 nM and 50 nM. For now, the most potentially effective inhibitors are the irreversible haloacetamidine compounds, e.g., F- and Cl-amidine, with IC_{50} ranging from 1.9 to 22 μM [19–22]. F- and Cl-amidine have been shown to be active against PAD4

* Corresponding author at: State Key Laboratory of Medicinal Chemical Biology, College of Pharmacy and Tianjin Key Laboratory of Molecular Drug Research, Nankai University, Haihe Education Park, 38 Tongyan Road, Tianjin, 300353, China.
** Corresponding authors.
E-mail addresses: jinj@nankai.edu.cn (J. Jin), dongmeili@nankai.edu.cn (D. Li), jianpinglin@nankai.edu.cn (J. Lin).
[1] These authors contributed equally to this work.

http://dx.doi.org/10.1016/j.jmgm.2016.11.016
1093-3263/

in vitro and cells [19,20]. Additionally, compound YW3-56, a Cl-amidine analog, with improved bioavailability was developed by Wang and co-workers [23]. Although the available PAD4 inhibitors increased dramatically in recently years, they are still far from developing the mechanism-based drug of PAD4. Therefore, it is necessary for developing novel and highly potent PAD4-specific inhibitors.

Recent years, in silico methods have been applied in identifying and developing new PAD4 inhibitors [24,25]. Teo et al. discovered three potential inhibitors of PAD4 through a structure-based virtual screening program, with IC_{50} values ranging from 1.54 to 2.50 mM [24]. In 2013, they discovered a moderately potent inhibitor for PAD4 (IC_{50} of 300 μM) using a ligand-based virtual screening [25]. Although the inhibition activity of PAD4 has not been dramatically improved comparing with known PAD4 inhibitors, it indicates that computational methods are effective way for discovery of PAD4 inhibitors.

Most of enzymes usually functionalize through a transition state (TS) pathway. Researches show that TS mimetics could bind to enzymes more tightly than substrates by stabilizing the conformation optimized through evolution for transition state formation [26,27]. Hence, TS mimetics have potential in discovery and development of drugs for several targets [26,28,29]. Although, it is difficulty to experimentally resolve the structure of the TS or high energy intermediates, TS structures derived from computational methods have been helpful for identification and development of new inhibitors acting as TS analogs [30]. Over the past decade, numerous TS mimetics have been developed as powerful enzymatic inhibitors by combining experimental and computational access to transition state information [30–40]. But the computational screening for TS mimics for PAD4 is still missing. Recently, we have elucidated the molecular mechanism of PAD4 inhibition by F-amidine through performing MD simulations and QM/MM calculations [41]. Our study showed that S_γ of thiolate Cys645 in the PAD4-F-amidine reactant complex initially attacked to $C\varsigma$ of F-amidine and formed a three-membered ring with $C\varsigma$ and C_η of F-amidine. Protonated His471 as proton donor was beneficial to helping F depart from fluoroacetamidine moiety of F-amidine. In this study, molecular dynamics simulation was carried out to explore the flexibility of protein on basis of the transition state geometry of PAD4 inhibited by F-amidine from our previous study [41]. Subsequently, a pharmacophore model was built acting as TS mimetics, which incorporated target flexibility based on the reaction mechanism. This pharmacophore model was applied to screen the National Cancer Institute database (NCI) and Enamine database. Further, compounds were docked against the active site of transition state geometry. Finally, two compounds out of 13 were found showing binding affinities to PAD4 with K_D values of 112 μM and 218 μM from SPR experiments and could potentially serve as PAD4 inhibitors.

2. Materials and methods

2.1. Molecular dynamics simulation and the selection of representative structures

The transition state complex of PAD4 inhibited by F-amidine from our previous study as in Fig. S1 was selected as the initial structure for molecular dynamics simulation (MD) [41]. The distances between the S_γ of Cys645 and the C_ζ and C_η of F-amidine, the F and C_η of F-amidine, the H of His471 and C_η of F-amidine were constrained during MD simulation to maintain the transition state geometry and further to consider the effect of the transition state on the conformational changes of PAD4. The complex was immersed in the center of a rectangular box of TIP3P water molecules with a buffer distance of 10 Å [42]. Neutralization of the system was achieved by adding seven Cl^- counter-ions. Then, the hydrogen atoms, the water and ions, the side chains and finally the entire system were minimized using steepest descent algorithm for the first 500 steps followed by conjugated gradient algorithm for the remaining steps. Then, the system was equilibrated for 1 ns. Finally, a 100 ns production run was performed under NPT (298.15 K and 1 atm).

The simulation was carried out with AMBER14 under periodic boundary conditions and the coordinates were stored to the trajectory every 2 ps [43]. The AMBER99SB force field was used to model the protein, while the force field parameters for F-amidine were created using general AMBER force field (GAFF) [44–46]. The SHAKE algorithm was employed to fix all bonds and the particle mesh Ewald (PME) method was applied to calculate the electrostatic contributions [47,48].

A total of 2084 snapshots were collected at 48 ps intervals from the MD trajectory [49]. Cluster analyses was performed with the average-linkage algorithm and residues within 8 Å of F-amidine were used in clustering to better represent the conformational changes within the active site [50]. 10 clusters were obtained and their representative structures of the transition state complex were further classified by comparing the root mean square deviation (RMSD) of the 8 Å residues. Finally, the 5 most divergent conformations were selected and used in the development of pharmacophore model.

2.2. Pharmacophore model generation and validation

Pharmacophore model features were generated using Protein-Ligand Interactions Fingerprints (PLIF) utility of Molecular Operation Environment (MOE) [51]. The PLIF method aims to capture the interactions between ligand and protein in complex using a fingerprint scheme. The water molecules and ions of the 5 most divergent complexes were removed and the complexes were aligned to each other. The interaction frequencies of individual residue with the ligand were recorded, and those present in 50% or more of the complexes were translated into pharmacophore elements. Excluded volumes were automatically generated to prevent clashes with receptor atoms in all complexes.

The Pharmacophore model was validated by a ligand dataset that contains 10 known PAD4 inhibitors (IC_{50} value < 23 μM) [22,52] (see Table S1 in Supporting information) and 1000 decoy ligands. The decoys that averaged 360 in molecular weight were downloaded from the Schrödinger website and their property distributions have been well characterized [53]. LigPrep was employed to expand tautomeric and ionization states for the ligands at pH 7.0 ± 2.0 [54]. Multiple conformations were generated using ConfGen heuristic search algorithm and an elimination criterion of 1.0 Å rmsd was used to remove redundant conformers [55]. The maximum relative energy difference of 10.0 kcal/mol was chosen to exclude high-energy structures. The standard enrichment factor (EF) and the area under curve (AUC) of ROC (Receiver operator characteristic curve) was analyzed to evaluate the performance of the pharmacophore model.

2.3. Molecular docking

Glide was employed to perform virtual screening and investigate the interactions between PAD4 and hits structures [56]. 5 representative conformations of the transition state complex from MD simulation were used to build the energy grid. The docking box center was set to the ligand (F-amidine). The scaling factor for van der Waals radii was set to 1.0. Default settings for the other parameters were used for both the grid generation and docking. The

molecules were ranked and selected for further study according to GlideScore.

2.4. Database screening and the selection of candidates

The pharmacophore models were used to screen the NCI (260,000 compounds) and Enamine database (300,000 compounds), using MOE. The NCI and Enamine molecules were prepared with the same procedure as the test ligand database described above. The ligands were ranked in order of their rmsd, a measure of how well the ligand matches the pharmacophore model elements. Those, with an rmsd lower than the selected cut-off value, were retained and docked to every of the 5 MD representative structures at the standard precision (SP) level with Glide. Glide docking study can further reduce the probability of picking false positives. The ligands have a high docking score in all of the 5 MD representative structures of the transition state complex were selected and visually inspected. Finally, the hits with some important interactions with the active site of PAD4 kept were subjected to SPR experiment to identify new and potential hits for future drug design.

2.5. Expression and purification of PAD4

PAD4 with N-terminal GST tag and PreScission Protease cleavage site downstream of the tag was expressed in BL21 (DE3) *E. coli*. Cells were harvested and homogenized in lysis buffer, containing 50 mM HEPES (*p*H 8.0), 500 mM NaCl and 1 mM DTT, followed by centrifugation (15,000 × *g*) at 4 °C. The fusion protein was purified through glutathione affinity chromatography and cleaved with PreSission protease at 4 °C overnight. The digested product was further purified with Hitrap Q anion exchange chromatogaphy and Superdex-200 gel filtration chromatography (GE Healthcare) to remove any contamination. The combinant proteins exceed 90% purity as detected by SDS-PAGE analysis.

2.6. SPR interaction assay

The PAD4 binding assay was based on Surface plasmon resonance (SPR) technique which was utilized for studying molecular interactions. We performed SPR experiments using a Biacore T200 optical biosensor (Biacore Life Sciences, GE Healthcare). The PAD4 was prepared in 10 mM sodium acetate (pH 5.0) and immobilized on a CM5 biosensor chip using standard amine coupling. Each compound was injected for 60 s and 300 s of dissociation time at a flow rate of 30 μL/min using in concentration series between 1 and 500 μM in running buffer (50 mm HEPES, pH 8.0, 300 mM NaCl, 2 mM DTT, 20 mM $CaCl_2$, and 5% DMSO). Raw data collected on an SPR biosensor require processing to eliminate systematic artifacts such as nonspecific binding, signal drift and discrepancies in buffer composition. All data was analyzed with the Biacore T200 Evaluation Software.

3. Results and discussion

3.1. Molecular dynamic simulation

Based on the transition state complex of PAD4 inhibited by F-amidine (Fig. S1), MD simulation was performed to investigate the conformational changes of PAD4 by constraining the reaction coordinates (as described in the Method section). The root mean square deviation (RMSD) of backbone atoms of the protein revealed that the transition state complex of PAD4 inhibited by F-amidine was stable with an average RMSD value of 1.5 Å (Fig. 1). And the total energy was also shown to be stable during the simulation time (Fig. S2). Thus, the convergent behavior of the transition state complex

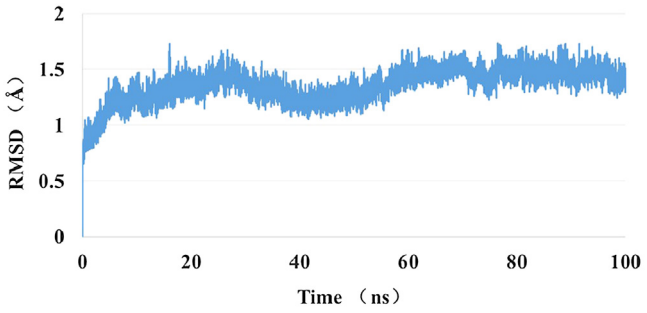

Fig. 1. RMSD values for backbone atoms of the transition state complex during the MD simulation.

system during simulation indicated that the results were reliable for the further studies.

To find the most representative structures of the transition state complex, 2084 snapshot structures were extracted from 100-ns molecular dynamics trajectory per 48 ps intervals and used to cluster the sampled phase space for transition state complex. In order to better sample the conformational changes, a total of 48 residues within 8 Å of F-amidine were selected to cluster the 2084 snapshots based on the RMSD values of atom positions (see Table S2). Then a total of 10 clusters were generated. The RMSD values of the representative structures of 10 clusters range from 0.656 to 1.42 Å (see Table S3). The representative structures of the transition state complex were further classified by comparing RMSD of the 8 Å residues. Finally, the 5 most divergent conformations were selected (see Fig. 2). These 5 representative conformations represented the flexibility of the transition state complex of PAD4 inhibited by F-amidine and were subsequently used to develop the pharmacophore model.

Fig. 2A showed 5 representative conformations of the transition state complex that were overlaid based on Cα superposition of active site residues. A comparison between the initial transition state complex from QM/MM calculation and the 5 representative conformations from MD simulation was made to identify the active site changes that were induced by transition state in enzyme reaction. The proposed citrullination mechanism of PAD4 indicated that two acidic residues Asp350 and Asp473 played an important role in maintaining the correct allocation of guanidine group in enzymatic cavity [57].

A detailed comparison demonstrated that Asp350 and Arg374 underwent large conformational changes in active site during the MD simulation compared to the initial transition state structure (Fig. 2B). The carboxyl group of Asp350 was perpendicular to the plane of acetamidine group in the initial transition state structure, but was parallel to the plane of acetamidine group in 4 representative conformations (cluster 1, cluster 3, cluster 8, and cluster 9). In addition, the carbonyl group of Asp350 formed two hydrogen bonds with the acetamidine group of F-amidine in 4 representative conformations, where only one hydrogen bond was observed in initial transition state structure. For 5 representative conformations, except cluster 9, the plane of the guanidinium group of Arg374 was perpendicular to the plane of the main chain amide of F-amidine. But the inherent flexibility of the Arg374 side chain has dramatically changed the orientations of hydrogen bond interaction with the main carbonyl of F-amidine. These 5 representative conformations from MD simulation have markedly different hydrogen bond directions by stabilizing the transition state structure and could lead to identify different ligand chemotypes during subsequently docking.

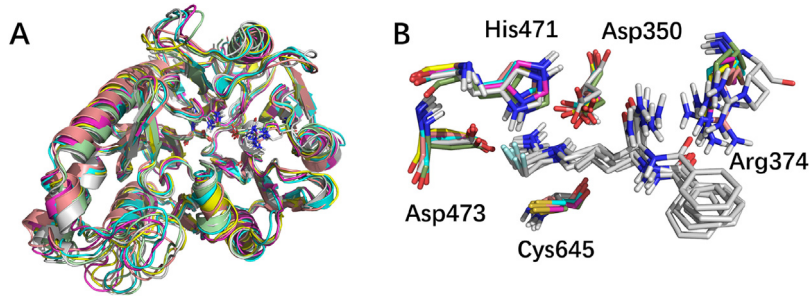

Fig. 2. (A) Overlay of 5 representative conformations of the transition state complex from MD snapshots. Green: cluster 0; Cyan: cluster 1; Magenta: cluster 3; Yellow: cluster 8; Orange: cluster 9; Gray: initial transition state. (B) F-amidine and the key residues in active site. (For interpretation of the references to colour in this figure legend, the reader is referred to the web version of this article.)

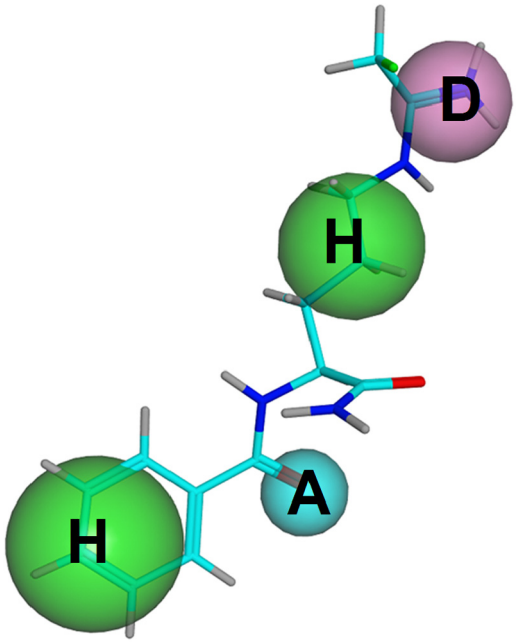

Fig. 3. Dynamic pharmacophore model derived from snapshots of MD simulation with starting structure of transition state complex. Green spheres: hydrophobic features (H); blue sphere: hydrogen bond acceptor (A); purple sphere: hydrogen bond donor (D). (For interpretation of the references to colour in this figure legend, the reader is referred to the web version of this article.)

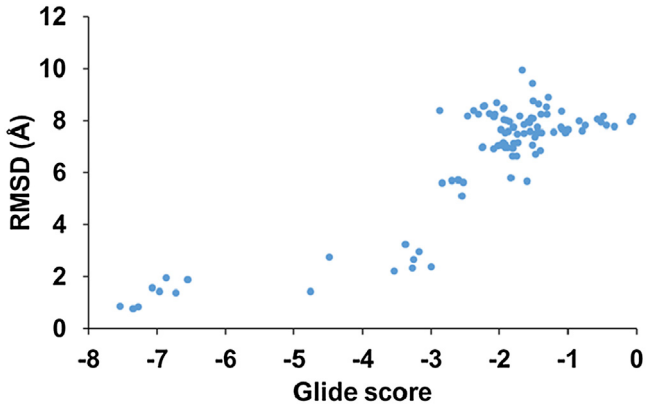

Fig. 4. RMSDs between 100 docking poses and transition state structure calculated by the Glide SP module.

3.2. Pharmacophore model generation and validation

To mimic key points in the reaction pathway for vs utilizing the reaction mechanism, a pharmacophore model was generated using the 5 representative conformations of the transition state complex of PAD4 inhibited by F-amidine obtained from the MD simulations snapshots. 5 representative conformations of the transition state complex were superimposed, and the common features shared by multiple states of the F-amidine were obtained by analyzing the fingerprints using PLIF module in MOE software. A pharmacophore model consisted of four features, including one hydrogen bond acceptor (A), one hydrogen bond donor (D), and two hydrophobic group (H) was generated depending on the interactions between F-amidine and key residues of the transition state complex of PAD4 inhibited by F-amidine. Seven key residues (Asp350, Arg374, His471, Asp473, Val469, Arg639, and Cys645) played a key role in keeping the ligand in correct position and orientation. Fig. 3 showed the pharmacophore model mapping with F-amidine. An amide group of F-amidine formed hydrogen-bond interaction with Arg374 in the active site and overlaid the hydrogen bond acceptor feature of pharmacophore model. In addition, the amine group of this compound formed hydrogen-bond interactions with Asp473 and Asp350 in the active site and mapped the hydrogen bond donor feature, and the aliphatic group that was involved in hydrophobic interaction with Val469 and Trp347 mapped the hydrophobic feature. Then the pharmacophore model can correctly reflect the interactions between PAD4 and its ligand.

A test dataset containing 10 inhibitors and 1000 decoys was used to evaluate the ability of transition state pharmacophore models to distinguish the inhibitors from the noninhibitors compounds. Roc analysis of the transition state pharmacophore model yielded AUC of 0.91. 40% of PAD4 inhibitors (4 of 10) were identified in the first 1% of the ranked dataset, whereas 60% of PAD inhibitors (6 of 10) were identified in the first 5% of the ranked dataset. Our results indicated that the pharmacophore model based on the transition state complex of PAD4 inhibited by F-amidine was reliable for recognizing inhibitors from noninhibitors and further virtual screening of chemical database.

3.3. Molecular docking study

To evaluate the reliability of the docking method, F-amidine was extracted from the transition state complex and redocked back to the same transition state structure. In this study, we used Glide SP scoring function to estimate protein-ligand binding affinities because it is faster and more tolerant to suboptimal fits than Glide XP [58]. Fig. 4 presented the plot of RMSDs between the transition state pose and the 100 docking poses against their docking scores. Fig. 4 showed that the docking scores were positively related to RMSDs. The worse glide scoring points were corresponding to the higher RMSDs regions in the plot, and conformations with better glide scores gave the lower RMSD values. In addition, docking is considered reliable if the RMSD value of the redocked pose is

less than 2 Å [59]. The 10 top poses with the top docking scores (<−6.0) showed their RMSDs below 2 Å, which indicated that Glide SP reproduced the transition state complex model well and was reliable to the PAD system.

To identify chemically stable molecules mimicking the features of bond lengths, angles, and electron density at the van der Waals surface of the actual transition state, 5 selected representative conformations from MD simulation were used for docking to screen candidate compounds that could tightly bind PAD4.

3.4. Database screening and the selection of candidates

As the pharmacophore screening was more efficient and faster than docking method, the pharmacophore model based on the transition state complex of PAD4 inhibited by F-amidine was used to screen the NCI (260,000 compounds) and Enamine database (300,000 compounds) firstly. Retrieved hits were required to match four pharmacophore features when screening the chemical database. Then a total of 4959 compounds mapped upon all of the pharmacophoric features were selected, when the minimum RMSD cutoff was set to 0.6. The workflow of database screening was shown in Fig. 5. Subsequently, 4959 compounds obtained from pharmacophore screening were further submitted to dock to every

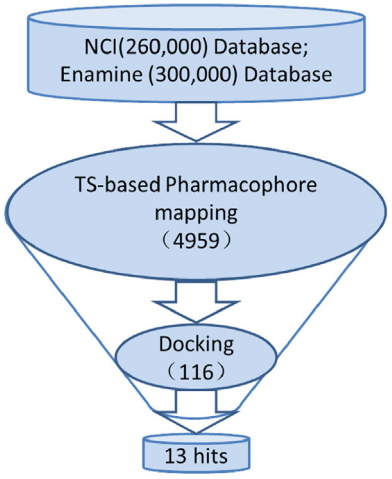

Fig. 5. Workflow of virtual screening.

of the 5 MD representative structures of the transition state complex of PAD4 inhibited by F-amidine using Glide SP. Then a total of 116 compounds remained after combining the results from the

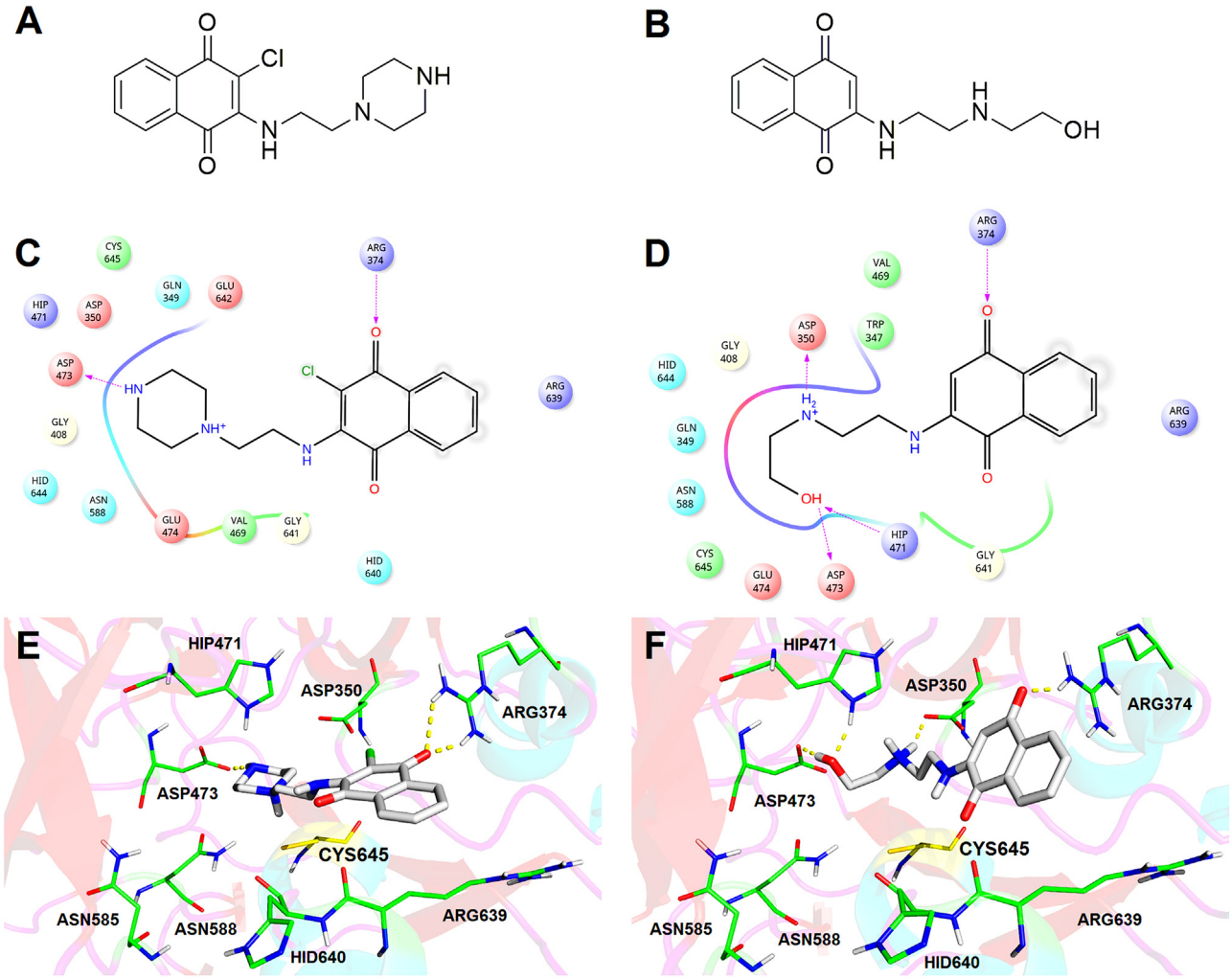

Fig. 6. The potential binding pose of 2 compounds with PAD4. Chemical structures of compound 2 (A) and compound 3 (B); two-dimensional ligand interaction diagrams of compound 2 (C) and compound 3 (D) (Residues are shown as dots and two hits are shown as line. Line and arrow in magenta represent hydrogen bond); the binding modes of compound 2 (E) and compound 3 (F) in the active site of PAD4 (PAD4 is represented in cartoon style. Two hits and residues are shown in sticks and lines, respectively. The yellow dotted line represents intermolecular hydrogen bond interaction). (For interpretation of the references to colour in this figure legend, the reader is referred to the web version of this article.)

Table 1
Glide scores, RMSD and K_D values of two hit compounds.

Compounds	Glide score	RMSD[a]	K_D[b] (μM)	LogP[c]	LLE(K_D)[d]	LE(K_D)[e]
2	−5.98	0.25	218	0.36	3.30	0.23
3	−6.70	0.39	112	−0.14	4.09	0.28

[a] RMSD:Root Mean Square Distance.
[b] K_D: Dissociation equilibrium constant. At this concentration 50% of all binding site are occupied.
[c] LogP: LogP was calculated using QikProp.
[d] LLE(K_D): pK_D − predicted log P.
[e] LE(KD): (1.37 × pK_D)/HA, HA denotes the number of non-hydrogen atoms.

five dockings with a docking score better or equal to −5. These 116 compounds were further visually inspected based on their docking poses by analyzing significant interactions with residues Trp347, Asp350, Arg374, and Asp473. Finally, 13 compounds (see Table S4) were selected as final candidates for the test of in vitro PAD4 SPR interaction assay.

3.5. SPR interaction analysis

The dissociation constants (K_D) of compounds binding to PAD4 were determined by SPR interaction assay. The binding affinities of compound 2 and 3 to PAD4 are in the micromolar range with K_D of 218 μM and 112 μM, respectively. Furthermore, these two compounds are of excellent water solubility. Compared with compound 2, compound 3 displayed much stronger binding affinity toward PAD4. Table 1 shows the correlation between binding affinity of hit compounds and docking scores and the RMSD values computed from the pharmacophore model. Table 1 indicated that compound 3 with K_D value of 112 μM displayed better docking score (-6.70) than compound 2. In addition, the ligand-lipophilic efficiency (LLE) and ligand efficiency (LE) were calculated based on K_D values for evaluating the quality and druglikeness of initial screening hits. LogP was calculated using QikProp[60]. The LogP values of compound 2 and 3 were 0.36 and −0.14, leading to the LLE values with 3.30 and 4.09, respectively. Generally, with LogP value of ∼2.5–3.0, an ideal LLE value is greater than 5 for an optimized drug candidate[61]. Table 1 showed that the LE values were comparable (0.23 and 0.28 for compound 2 and 3, respectively). In a lead optimization, ligand efficiency is considered to be a good metric for dealing with molecular size[62]. Therefore, these two compounds could be further optimized based on lipophilicity and molecular mass to generate high activity leads.

3.6. Analysis of hit compounds

The 2D structures of compound 2 and 3 were showed in Fig. 6A and B, respectively. These two compounds were found to have the same scaffold structure (naphthoquinone). To illustrate the structure-activity relationship between PAD4 and the hits, the possible interaction modes of compound 2 and 3 with PAD4 in docking modes were presented in Fig. 6C–F. We can see that the binding modes and interactions of compound 2 and 3 with PAD4 are similar with that of F-amidine. The piperazine ring of compound 2 forms hydrogen bond with Asp473 in the active site, and 2-chloro-naphthoquinone group of compound 2 points to the solvent accessible region and forms hydrogen bond with Arg374 (Fig. 6C and E). Fig. 6D and F demonstrate that the hydroxyl group of compound 3 forms two hydrogen bonds with His471 and Asp473, the secondary amine motif forms a hydrogen bond with Asp350. And the naphthoquinone group of compound 3 points to the solvent accessible region and forms one hydrogen bond with Arg374. Thus, the interactions with key residues (Asp350, Arg374, His471 and Asp473) are required in the design of potent inhibitors of PAD4. These two compounds could be further developed into PAD4 inhibitors through chemical modifications.

4. Conclusion

In this study, we have investigated the flexibility of protein on basis of the transition state geometry of PAD4 inhibited by F-amidine from QM/MM calculation. In order to explore the effect of the transition state on the conformational changes of PAD4, the distances between the Sγ of Cys645 and the Cζ and Cη of F-amidine, the F and Cη of F-amidine, the H of His471 and Cη of F-amidine were constrained during MD simulation to maintain the transition state geometry. Then 5 representative conformations of the transition state complex were obtained after clustering MD trajectories. We found that Asp350 and Arg374 underwent large conformational changes in active site during the MD simulation compared to the initial transition state structure resulting in markedly different hydrogen bond directions with F-amidine. To mimic key points in the reaction pathway, and a pharmacophore model containing four features by using 5 representative structures was generated. Virtual screening was performed using the pharmacophore model and molecular docking for retrieving chemically stable molecules mimicking the features of actual transition state. Two of 13 compounds with K_D values of 112 μM and 218 μM (from SPR experiments) were retrieved from NCI database. These two molecules could potentially serve as PAD4 inhibitors. On the whole, the presented method is a useful alternative to traditional methods for screening and identifying new scaffolds of enzyme inhibitors.

Acknowledgments

We thank Dr. Jie Shen from College of Pharmacy, Nankai University for insightful discussion. And this study was supported by National Basic Research Program (973 Program, No. 2013CB911100) and National Natural Science Foundation of China (NSFC, No. 21203101).

Appendix A. Supplementary data

Supplementary data associated with this article can be found, in the online version, at http://dx.doi.org/10.1016/j.jmgm.2016.11.016.

References

[1] J. Jones, C. Causey, B. Knuckley, J.L. Slack-noyes, R. Paul, Protein arginine deiminase 4 (PAD4): current understanding and future therapeutic potential, Curr. Opin. Drug. Discov. Devel. 12 (2013) 616–627.
[2] E.R. Vossenaar, a. J.W. Zendman, W.J. Van Venrooij, G.J.M. Pruijn, PAD, a growing family of citrullinating enzymes: Genes, features and involvement in disease, Bioessays 25 (2003) 1106–1118, http://dx.doi.org/10.1002/bies.10357.
[3] K.L. Bicker, P.R. Thompson, The protein arginine deiminases: structure, function, inhibition, and disease, Biopolymers 99 (2013) 155–163, http://dx.doi.org/10.1002/bip.22127.

[4] S. Muller, M. Radic, Citrullinated autoantigens: from diagnostic markers to pathogenetic mechanisms, Clin. Rev. Allergy Immunol. 49 (2015) 232–239, http://dx.doi.org/10.1007/s12016-014-8459-2.
[5] C. Foulquier, M. Sebbag, C. Clavel, S. Chapuy-Regaud, R. Al Badine, M.C. Méchin, C. Vincent, R. Nachat, M. Yamada, H. Takahara, M. Simon, M. Guerrin, G. Serre, Peptidyl arginine deiminase type 2 (PAD-2) and PAD-4 but not PAD-1, PAD-3, and PAD-6 are expressed in rheumatoid arthritis synovium in close association with tissue inflammation, Arthritis Rheum. 56 (2007) 3541–3553, http://dx.doi.org/10.1002/art.22983.
[6] A. Suzuki, R. Yamada, X. Chang, S. Tokuhiro, T. Sawada, M. Suzuki, M. Nagasaki, M. Nakayama-Hamada, R. Kawaida, M. Ono, M. Ohtsuki, H. Furukawa, S. Yoshino, M. Yukioka, S. Tohma, T. Matsubara, S. Wakitani, R. Teshima, Y. Nishioka, A. Sekine, A. Iida, A. Takahashi, T. Tsunoda, Y. Nakamura, K. Yamamoto, Functional haplotypes of PADI4, encoding citrullinating enzyme peptidylarginine deiminase 4, are associated with rheumatoid arthritis, Nat. Genet. 34 (2003) 395–402, http://dx.doi.org/10.1038/ng1206.
[7] J.M. Kahlenberg, D.A. Fox, Advances in the Medical Treatment of Rheumatoid Arthritis, Hand. Clin. 27 (2011) 11–20, http://dx.doi.org/10.1016/j.hcl.2010.09.002.
[8] J.S. Smolen, G. Steiner, Therapeutic strategies for rheumatoid arthritis, Nat. Rev. Drug Discov. 2 (2003) 473–488, http://dx.doi.org/10.1038/nrd1109.
[9] T.T. Mottonen, P.J. Hannonen, M. Boers, Combination DMARD therapy including corticosteroids in early rheumatoid arthritis, Clin. Exp. Rheumatol. 17 (1999) S59–S65.
[10] H. Van Dongen, J. Van Aken, L.R. Lard, K. Visser, H.K. Ronday, H.M.J. Hulsmans, I. Speyer, M.L. Westedt, A.J. Peeters, C.F. Allaart, R.E.M. Toes, F.C. Breedveld, T.W.J. Huizinga, Efficacy of methotrexate treatment in patients with probable rheumatoid arthritis: a double-blind, randomized, placebo-controlled trial, Arthritis Rheum. 56 (2007) 1424–1432, http://dx.doi.org/10.1002/art.22525.
[11] J.M. Cash, J.H. Klippel, Second-line drug therapy for rheumatoid arthritis, N. Engl. J. Med. 330 (1994) 1368–1375.
[12] T. Kouzarides, Chromatin modifications and their function, Cell 128 (2007) 693–705, http://dx.doi.org/10.1016/j.cell.2007.02.005.
[13] K. Arita, H. Hashimoto, T. Shimizu, K. Nakashima, M. Yamada, M. Sato, Structural basis for Ca2+-induced activation of human PAD4, Nat. Struct. Mol. Biol. 11 (2004) 777–783, http://dx.doi.org/10.1038/nsmb799.
[14] D.J. Slade, P.F. Fang, C.J. Dreyton, Y. Zhang, J. Fuhrmann, D. Rempel, B.D. Bax, S.A. Coonrod, H.D.M. Lewis, M.L. Guo, Gross and P. R. Thompson, Protein Arginine Deiminase 2 Binds Calcium in an Ordered Fashion: Implications for Inhibitor Design, ACS. Chem. Biol. 10 (2015) 1043–1053, http://dx.doi.org/10.1021/cb500933j.
[15] H.D. Lewis, J. Liddle, J.E. Coote, S.J. Atkinson, M.D. Barker, B.D. Bax, K.L. Bicker, R.P. Bingham, M. Campbell, Y.H. Chen, C. Chung, P.D. Craggs, R.P. Davis, D. Eberhard, G. Joberty, K.E. Lind, K. Locke, C. Maller, K. Martinod, C. Patten, O. Polyakova, C.E. Rise, M. Rüdiger, R.J. Sheppard, D.J. Slade, P. Thomas, J. Thorpe, G. Yao, G. Drewes, D.D. Wagner, P.R. Thompson, R.K. Prinjha, D.M. Wilson, Inhibition of PAD4 activity is sufficient to disrupt mouse and human NET formation, Nat. Chem. Biol. 11 (2015) 189–191, http://dx.doi.org/10.1038/nchembio.1735.
[16] L.B. Pritzker, M.A. Moscarello, A novel microtubule independent effect of paclitaxel: the inhibition of peptidylarginine deiminase from bovine brain, Biochim. Biophys. Acta. 1388 (1998) 154–160, http://dx.doi.org/10.1016/S0167-4838(98)00175-7.
[17] B. Knuckley, Y. Luo, P.R. Thompson, Profiling protein arginine deiminase 4 (PAD4): a novel screen to identify PAD4 inhibitors, Bioorg. Med. Chem. 16 (2008) 739–745, http://dx.doi.org/10.1016/j.bmc.2007.10.021.
[18] E.M. Stone, T.H. Schaller, H. Bianchi, M.D. Person, W. Fast, Inactivation of two diverse enzymes in the amidinotransferase superfamily by 2-chloroacetamidine: dimethylargininase and peptidylarginine deiminase, Biochemistry 44 (2005) 13744–13752, http://dx.doi.org/10.1021/bi051341y.
[19] Y. Luo, B. Knuckley, Y.-H. Lee, M.R. Stallcup, P.R. Thompson, A fluoroacetamidine-based inactivator of protein arginine deiminase 4: design, synthesis, and in vitro and in vivo evaluation, J. Am. Chem. Soc. 128 (2006) 1092–1093, http://dx.doi.org/10.1021/ja0576233.
[20] Y. Luo, K. Arita, M. Bhatia, B. Knuckley, Y.H. Lee, M.R. Stallcup, M. Sato, P.R. Thompson, Inhibitors and inactivators of protein arginine deiminase 4: Functional and structural characterization, Biochemistry 45 (2006) 11727–11736, http://dx.doi.org/10.1021/bi061180d.
[21] J.E. Jones, J.L. Slack, P. Fang, X. Zhang, V. Subramanian, C.P. Causey, S. a. Coonrod, M. Guo, P.R. Thompson, Synthesis and screening of a haloacetamidine containing library to identify PAD4 selective inhibitors, ACS Chem. Biol. 7 (2012) 160–165, http://dx.doi.org/10.1021/cb200258q.
[22] C.P. Causey, J.E. Jones, J.L. Slack, D. Kamei, L.E. Jones, V. Subramanian, B. Knuckley, P. Ebrahimi, A. a. Chumanevich, Y. Luo, H. Hashimoto, M. Sato, L.J. Hofseth, P.R. Thompson, The development of N-α −(2-Carboxyl)benzoyl- n 5 -(2-fluoro-1-iminoethyl)- l -ornithine amide (o -F-amidine) and N-α −(2-Carboxyl)benzoyl- N 5 -(2-chloro-1-iminoethyl)- l -ornithine amide (o -Cl-amidine) as second generation protein arginine deiminase, J. Med. Chem. 54 (2011) 6919–6935, http://dx.doi.org/10.1021/jm2008985.
[23] Y. Wang, P. Li, S. Wang, J. Hu, X.A. Chen, J. Wu, M. Fisher, K. Oshaben, N. Zhao, Y. Gu, D. Wang, G. Chen, Y. Wang, Anticancer peptidylarginine deiminase (PAD) inhibitors regulate the autophagy flux and the mammalian target of rapamycin complex 1 activity, J. Biol. Chem. 287 (2012) 25941–25953, http://dx.doi.org/10.1074/jbc.M112.375725.
[24] C.Y. Teo, S. Shave, A.L.T. Chor, A.B. Salleh, M.B.B.A. Rahman, M.D. Walkinshaw, B.A. Tejo, Discovery of a new class of inhibitors for the protein arginine deiminase type 4 (PAD4) by structure-based virtual screening, BMC Bioinf. 13 (2012) S4, http://dx.doi.org/10.1186/1471-2105-13-S17-S4.
[25] M. Basyaruddin, C. Rahman, Ligand-based virtual screening for the discovery of inhibitors for protein arginine deiminase type 4 (PAD4), J. Postgenomics Drug Biomark. Dev. 03 (2013) 1–5, http://dx.doi.org/10.4172/2153-0769.1000118.
[26] V.L. Schramm, Transition states, analogues, and drug development, ACS Chem. Biol. 8 (2013) 71–81, http://dx.doi.org/10.1021/cb300631k.
[27] R. Wolfenden, Transition state analog inhibitors and enzyme catalysis, Annu. Rev. Biophys. Bioeng. 5 (1976) 271–306.
[28] V.L. Schramm, Enzymatic transition states, transition-State analogs, dynamics, thermodynamics, and lifetimes, Annu. Rev. Biochem. 80 (2011) 703–732, http://dx.doi.org/10.1146/annurev-biochem-061809-100742.
[29] R. Wolfenden, Conformational aspects of inhibitor design: enzyme–substrate interactions in the transition state, Bioorg. Med. Chem. 7 (1999) 647–652, http://dx.doi.org/10.1016/S0968-0896(98)00247-8.
[30] F. Svensson, K. Engen, T. Lundbäck, M. Larhed, C. Sköld, Virtual screening for transition state analogue inhibitors of IRAP based on quantum mechanically derived reaction coordinates, J. Chem. Inf. Model. 55 (2015) 1984–1993, http://dx.doi.org/10.1021/acs.jcim.5b00359.
[31] a. K. Mahalingam, L. Axelsson, J.K. Ekegren, J. Wannberg, J. Kihlström, T. Unge, H. Wallberg, B. Samuelsson, M. Larhed, A. Hallberg, HIV-1 protease inhibitors with a transition-state mimic comprising a tertiary alcohol: improved antiviral activity in cells, J. Med. Chem. 53 (2010) 607–615, http://dx.doi.org/10.1021/jm901165g.
[32] S. Cha, R.P. Agarwal, R.E. Parks, Tight-binding inhibitors—II, Biochem. Pharmacol. 24 (1975) 2187–2197, http://dx.doi.org/10.1016/0006-2952(75)90051-9.
[33] S. Wang, A.M. Haapalainen, F. Yan, Q. Du, P.C. Tyler, G.B. Evans, A. Rinaldo-Matthis, R.L. Brown, G.E. Norris, S.C. Almo, V.L. Schramm, A picomolar transition state analogue inhibitor of MTAN as a specific antibiotic for helicobacter pylori, Biochemistry 51 (2012) 6892–6894, http://dx.doi.org/10.1021/bi3009664.
[34] K. Clinch, G.B. Evans, R.F.G. Fröhlich, S.A. Gulab, J.A. Gutierrez, J.M. Mason, V.L. Schramm, P.C. Tyler, A.D. Woolhouse, Transition state analogue inhibitors of human methylthioadenosine phosphorylase and bacterial methylthioadenosine/S-adenosylhomocysteine nucleosidase incorporating acyclic ribooxacarbenium ion mimics, Bioorg. Med. Chem. 20 (2012) 5181–5187, http://dx.doi.org/10.1016/j.bmc.2012.07.006.
[35] J.I. Ehrlich, V.L. Schranmm, Electrostatic potential surface analysis of the transition state for AMP nucleosidase and for formycin 5′-phosphate, a transition-state inhibitor, Biochemistry 33 (1994) 8890–8896, http://dx.doi.org/10.1021/bi00196a005.
[36] R.W. Miles, P.C. Tyler, R.H. Furneaux, C.K. Bagdassarian, V.L. Schramm, One-third-the-sites transition-state inhibitors for purine nucleoside phosphorylase, Biochemistry 37 (1998) 8615–8621, http://dx.doi.org/10.1021/bi980658d.
[37] G.B. Evans, R.H. Furneaux, V.L. Schramm, V. Singh, P.C. Tyler, Targeting the polyamine pathway with transition-state analogue inhibitors of 5′-methylthioadenosine phosphorylase, J. Med. Chem. 47 (2004) 3275–3281, http://dx.doi.org/10.1021/jm0306475.
[38] J.A. Gutierrez, M. Luo, V. Singh, L. Li, R.L. Brown, G.E. Norris, G.B. Evans, R.H. Furneaux, P.C. Tyler, G.F. Painter, D.H. Lenz, V.L. Schramm, Picomolar inhibitors as transition-state probes of 5′-methylthioadenosine nucleosidases, ACS Chem. Biol. 2 (2007) 725–734, http://dx.doi.org/10.1021/cb700166z.
[39] G.C. Zhou, S.L. Parikh, P.C. Tyler, G.B. Evans, R.H. Furneaux, O.V. Zubkova, P.A. Benjes, V.L. Schramm, Inhibitors of ADP-ribosylating bacterial toxins based on oxacarbenium ion character at their transition states, J. Am. Chem. Soc. 126 (2004) 5690–5698, http://dx.doi.org/10.1021/ja038159+.
[40] V. Singh, G.B. Evans, D.H. Lenz, J.M. Mason, K. Clinch, S. Mee, G.F. Painter, P.C. Tyler, R.H. Furneaux, J.E. Lee, P.L. Howell, V.L. Schramm, Femtomolar transition state analogue inhibitors of 5′-methylthioadenosine/S-adenosylhomocysteine nucleosidase from Escherichia coli, J. Biol. Chem. 280 (2005) 18265–18273, http://dx.doi.org/10.1074/jbc.M414472200.
[41] D. Li, C. Liu, J. Lin, Theoretical study of the mechanism of protein arginine deiminase 4 (PAD4) inhibition by F-amidine, J. Mol. Graph. Model. 55 (2015) 25–32, http://dx.doi.org/10.1016/j.jmgm.2014.10.014.
[42] W.L. Jorgensen, J. Chandrasekhar, J.D. Madura, R.W. Impey, M.L. Klein, Comparison of simple potential functions for simulating liquid water, J. Chem. Phys. 79 (1983) 926, http://dx.doi.org/10.1063/1.445869.
[43] D.A. Pearlman, D.A. Case, J.W. Caldwell, W.S. Ross, T.E. Cheatham, S. DeBolt, D. Ferguson, G. Seibel, P.A. Kollman, AMBER, a package of computer programs for applying molecular mechanics, normal mode analysis, molecular dynamics and free energy calculations to simulate the structural and energetic properties of molecules, Comput. Phys. Commun. 91 (1995) 1–41, http://dx.doi.org/10.1016/0010-4655(95)00041-D.
[44] W.D. Cornell, P. Cieplak, C.I. Bayly, I.R. Gould, K.M. Merz, D.M. Ferguson, D.C. Spellmeyer, T. Fox, J.W. Caldwell, P.A. Kollman, A second generation force field for the simulation of proteins, nucleic acids, and organic molecules, J. Am. Chem. Soc. 117 (1995) 5179–5197, http://dx.doi.org/10.1021/ja00124a002.
[45] P. Rezácová, D. Borek, S.F. Moy, A. Joachimiak, Z. Otwinowski, Crystal structure and putative function of small Toprim domain-containing protein from Bacillus stearothermophilus, Proteins 70 (2008) 311–319, http://dx.doi.org/10.1002/prot.

[46] J.M. Wang, R.M. Wolf, J.W. Caldwell, P.a. Kollman, D.a. Case, Development and testing of a general amber force field, J. Comput. Chem. 25 (2004) 1157–1174, http://dx.doi.org/10.1002/jcc.20035.
[47] J.-P. Ryckaert, G. Ciccotti, H.J. Berendsen, Numerical integration of the cartesian equations of motion of a system with constraints: molecular dynamics of n-alkanes, J. Comput. Phys. 23 (1977) 327–341, http://dx.doi.org/10.1016/0021-9991(77)90098-5.
[48] U. Essmann, L. Perera, M.L. Berkowitz, T. Darden, H. Lee, L.G. Pedersen, A smooth particle mesh Ewald method, J. Chem. Phys. 103 (1995) 8577–8593, http://dx.doi.org/10.1063/1.470117.
[49] A.L. Bowman, A. Makriyannis, Approximating protein flexibility through dynamic pharmacophore models: application to fatty acid amide hydrolase (FAAH), J. Chem. Inf. Model. 51 (2011) 3247–3253, http://dx.doi.org/10.1021/ci200371z.
[50] P.B. Burger, Development of a Dynamic Receptor-based Pharmacophore Model of Plasmodium Falciparum Spermidine Synthase for Selective Inhibitor Identification, University of Pretoria, 2009.
[51] Molecular Operating Environment (MOE), 2013.08; Chemical Computing Group Inc., 1010 Sherbooke St. West, Suite #910, Montreal,QC, Canada,H 3A 2R7, 2016 (n.d.).
[52] B. Knuckley, J.E. Jones, D.a. Bachovchin, J. Slack, C.P. Causey, S.J. Brown, H. Rosen, B.F. Cravatt, P.R. Thompson, A fluopol-ABPP HTS assay to identify PAD inhibitors, Chem. Commun. (Camb) 46 (2010) 7175–7177, http://dx.doi.org/10.1039/c0cc02634d.
[53] Schrodinger Suite 2013 Protein preparation Wizard; Epik Version 2.6, Schrodinger, LLC, New York, NY, 2013; Impact Version 6.1, Schrodinger, LLC, New York, NY, 2013; Prime Version 3.3, Schrodinger, LLC, New York, NY, 2013 (n.d.).
[54] LigPrep, Version 2.8, Schrodinger, LLC, New York, NY, 2013 (n.d.).
[55] ConfGen, Version 2.6, Schrodinger, LLC, New York, NY, 2013 (n.d.).
[56] Glide, Version 6.1, Schrodinger, LLC, New York, NY, 2013 (n.d.).
[57] P.L. Kearney, M. Bhatia, N.G. Jones, L. Yuan, M.C. Glascock, K.L. Catchings, M. Yamada, P.R. Thompson, Kinetic characterization of protein arginine deiminase 4: a transcriptional corepressor implicated in the onset and progression of rheumatoid arthritis, Biochemistry 44 (2005) 10570–10582, http://dx.doi.org/10.1021/bi050292m.
[58] N.K. Salam, R. Nuti, W. Sherman, Novel method for generating structure-based pharmacophores using energetic analysis, J. Chem. Inf. Model. 49 (2009) 2356–2368, http://dx.doi.org/10.1021/ci900212v.
[59] A.N. Jain, Bias, reporting, and sharing: computational evaluations of docking methods, J. Comput. Aided. Mol. Des. 22 (2008) 201–212, http://dx.doi.org/10.1007/s10822-007-9151-x.
[60] QikProp, version 3.8, Schrödinger, LLC, New York, NY, 2013., (n.d.).
[61] P.D. Leeson, B. Springthorpe, The influence of drug-like concepts on decision-making in medicinal chemistry, Nat. Rev. Drug Discov. 6 (2007) 881–890, http://dx.doi.org/10.1038/nrd2445.
[62] A.L. Hopkins, G.M. Keserü, P.D. Leeson, D.C. Rees, C.H. Reynolds, The role of ligand efficiency metrics in drug discovery, Nat. Rev. Drug Discov. 13 (2014) 105–121, http://dx.doi.org/10.1038/nrd4163.